

UNIFORM RIBBON-BEAM GENERATION FOR ACCELERATOR  
PRODUCTION OF TRITIUM\*

Andrew J. Jason, Barbara Blind, Ernest M. Svaton†  
MS H808, Los Alamos National Laboratory, Los Alamos, NM 87545

**Abstract**

A scheme has been developed to produce a uniform distribution of beam energy over the large target of a tritium production facility. A highly expanded ribbon beam is produced by an astigmatic lens system that contains strong octupole and duodecapole elements. The nonlinear focusing of these elements gives rise to a nearly uniform distribution of intensity along most of the ribbon length. Sweeping the beam orthogonal to the ribbon then provides a simplified alternative to two-dimensional raster schemes. Additionally, the scheme virtually eliminates the beam fringes by deflecting fringe particles into the beam core. This scheme reduces transport line activation and allows a decreased element size. The technique can be used in other applications that require a uniform intensity distribution in one dimension. Further work is continuing on producing an analogously two-dimensionally uniform beam.

**Introduction**

The stratagem of the accelerator production of tritium (APT) requires impingement of an intense linac-produced proton beam (approaching a gigawatt in continuous power—we have assumed 400 mA at 2 GeV) onto a beam stop for production of neutrons, which in turn transform a lithium target into tritium. To optimize this process under the constraints of heat and neutron transport as well as material properties, illumination of the beam stop must be relatively uniform. Additionally, the beam must be greatly expanded to approximately 4 meters square from its original millimeter dimensions at the linac. To preserve a small aperture at the entrance of the beam-stop housing, required for minimization of neutron escapes and to maintain reasonable housing dimensions, the expansion half-angle must be greater than about 10°.

It would not be appropriate to simply expand the beam by an appropriate linear optical system because the Gaussian-like intensity distribution characteristic of linacs would be sharply peaked at the beam stop with appreciable intensity at several times its rms radius. An alternative scheme would raster a beam, expanded to a diameter of perhaps several centimeters, over the beam stop in a two dimensional scan. Thermal considerations dictate an ~ 1-Hz minimum frequency in the direction of slowest scan. The corresponding minimum rate perpendicular to this dimension would then be ~10 Hz. The most straightforward implementation of the raster scheme would involve two dipole magnets that, serially along the transport line, scan the beam at 10 Hz in the horizontal direction and 1 Hz in the vertical. A straightforward estimate of magnet properties shows that very large apertures are needed to clear the deflected beam and that magnet reactive EMFs are quite large. For the larger magnet, run at 1 Hz, we estimate that a 1.3 m square aperture is necessary, implying exterior dimensions of 3-by 4-m cross section and 1.2 m length. The peak reactive EMF would be about 22 kV. Additionally, to maintain uniform target illumination the magnets cannot be run in a first-harmonic mode but must be energized with several harmonics or use very high power switching devices. Other schemes such as mechanically rotating the scanning magnets or sweeping the beam energy have proved even less practical.

We suggest instead a technique that forms a narrow ribbon beam, uniform in intensity along most of its length. Uniform beam-stop illumination would then be automatically accomplished in one dimension and the beam swept at a low rate in the other, using a single dipole magnet that is smaller than those for the raster scheme. Such a beam is produced by the influence of nonlinear optics elements, octupoles and duodecapoles, which distort the beam phase-space distribution in a manner that folds the beam edges onto its center. In addition to providing a relatively uniform distribution, the beam is well contained with very low fringe intensity.

**One-Dimensional Calculation**

Consider a beam, convergent in the x-direction and appropriately focused to remain small in the y-direction. The beam is passed through an octupole magnet, passes through a waist, and then continues expanding to the beam stop. Particle motion in the octupole obeys the differential equations

$$\begin{aligned} x'' &= \frac{B_o}{r_o^3 B_p} (x^3 - 3xy^2) \\ y'' &= -\frac{B_o}{r_o^3 B_p} (y^3 - 3x^2y) \end{aligned} \tag{1}$$

where  $B_o$  is the octupole pole-tip field,  $r_o$  the pole-tip radius, and  $B_p$  the beam rigidity. The double primes on x and y indicate second derivatives with respect to the direction of travel, the z-axis. Because we have arranged for the beam to be small in the y-direction during its passage through the octupole (e.g., by arranging a y-waist at this point), the terms in Eq. (1) that contain powers of y as factors can be neglected. Integrating Eq. (1) under these assumptions gives the effect of the octupole on the particle divergence,  $x'$ , for a short octupole of length  $\ell$  as

$$\delta x' = T_{2,111} x^3 + 0(y, \ell^2 \dots) = \frac{B_o \ell}{r_o^3 B_p} x^3 + \dots \tag{2}$$

Here  $T_{2,111}$  is the third-order octupole matrix element relating  $x'$  to  $x^3$ . There are 40 such elements; all but  $T_{2,111}$  are coefficients of powers of y or are of order  $\ell^2$  or smaller. Hence the beam is unaffected in the y-direction because of its small size and the effect in the x-direction is given by Eq. (2), neglecting the first-order drift-like character of the octupole. Just before passage through the octupole, the beam may be represented by a straight line on a phase-space plot as in Fig. 1a. This representation is justified if we have expanded the beam sufficiently in both x and x' with respect to the scale of its emittance. After passage through the octupole, the beam will be described by the relation

$$x'_o = Ax_o + Bx_o^3 \tag{3}$$

where A describes the tilt of the beam before the octupole (a negative number in our case because the beam is converging) and B is the coefficient of  $x^3$  in Eq. (2). This relationship is also plotted in Fig. 1a. Figure 1b shows an

\*Work performed under the auspices of the U.S. Department of Energy, Defense Programs.

†Rocketdyne Division, Rockwell International, Canoga Park, CA

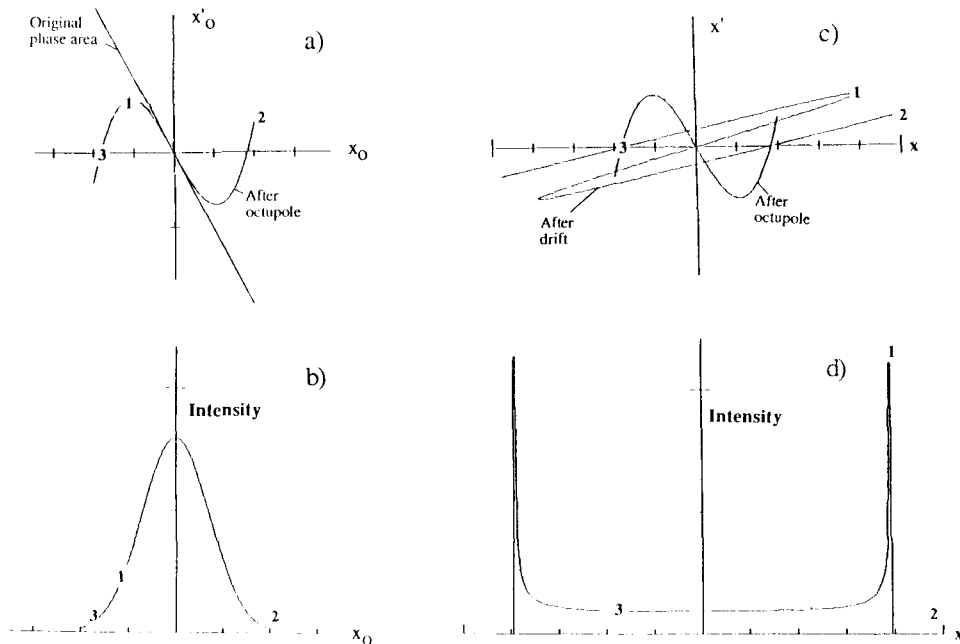


Fig.1. Phase-space diagrams and intensity distributions calculated, using a one-dimensional model, for a transport line, consisting of an octupole and a drift, calculated using a one-dimensional model. In a) the initial beam is distorted by an octupole field. Its Gaussian intensity distribution is shown in b). Evolution through a drift produces the phase space area shown in c) and the distribution shown in d). The scale of the plots is arbitrary.

assumed (Gaussian) intensity distribution plotted to the 3 rms ( $3\sigma$ ) extremes. We follow its evolution through the drift from the octupole to the beam stop. As an aid to this, three particles in the beam are numbered in Fig. 1. With the above assumptions and neglecting space charge effects, the relations describing particle evolution through a drift space  $L$  are

$$\begin{aligned} x &= x_o + x'_o L \\ x' &= x'_o \end{aligned} \quad (4)$$

The influence of the octupole does not immediately change the beam distribution in  $x$ . However, the phase-space distribution and subsequent evolution is strongly altered. Particle 3, having zero divergence, remains fixed on the  $x$ -axis. Particle 1 is at a divergence extremum and hence progresses toward positive values of  $x$ . After some drift, the converging beam forms a waist. Particle 1 crosses the  $z$ -axis near this waist. The size of the waist is substantially broadened by the octupole presence, thus diminishing space-charge effects at this point. After further drift, the situation in Fig. 1c applies. The beam has expanded proportionally to the drift length after the waist, and particle 1 is at a radius nearly four times its original radius. The important feature of the motion is that particle 1 has nearly caught up with particle 2, originally at the  $3\sigma$  extreme considered. Hence, the core of the beam has enveloped and contained the fringes. The intensity distribution at this point is shown in Fig. 1d. The evolution of the distribution was calculated by dividing the original distribution into small intervals, mapping each interval into its downstream phase space coordinates by relations (4) while conserving probability for each interval, and then summing over the three branches evident in the beam phase-space distribution.

The intensity distribution in Fig. 1d is relatively flat except at the edges where the fold in beam phase space is projected onto the spatial axis as cusps. With further drift, point 1 would overtake point 2 and incorporate all the beam lying within more than  $3\sigma$  of the original distribution into the core, leaving less than 0.3% of the beam in a widely scattered halo. The amount of beam

captured can be improved somewhat with optimization, but it is possible to capture the fringes to approximately 5% (0.0001% fringe population) by adding nonlinear elements with higher odd multiplicities. For example, the addition of a properly dimensioned duodecapole (field variation as  $x^5$ ) of opposite sign to the octupole significantly decreases the value of  $x'_o$  for parts of the beam at and beyond  $3\sigma$ . Hence, the region in Fig. 1a for which particle divergences are less in magnitude than the  $x'$  extremum (and therefore lie within the capture region) is expanded.

### Three-Dimensional Calculation

In obtaining the results of the previous section, we have assumed negligible beam emittance, zero octupole length, negligible space-charge effects, and an arbitrary scale. To demonstrate the feasibility of the technique, we have taken a pulsed beam with transverse rms lab emittances  $\epsilon = 0.003 \pi \text{ cm} \cdot \text{mrad}$ , typical of a low-emittance linac, and expanded it by a quadruplet lens configuration to  $\sigma = 4 \text{ cm}$  in the  $x$ -direction and  $\sigma = 1 \text{ mm}$  in the  $y$ -direction. The rms  $x$ -divergence was 17 mrad, and the beam was slightly convergent in  $y$  at 0.1 mrad. The final results are very insensitive to the initial emittance; increases of over a factor of 100 in  $\epsilon$  cause negligible changes in the result. Using the third-order code MARYLIE<sup>1</sup>, we optimized the configuration shown in Fig. 2, which consists of an octupole and a quadrupole doublet to produce a beam with an  $x$ -waist downstream of the F quad and a divergence for the beam extrema in  $x'$  (corresponding to point 1 in Fig. 1) of  $12^\circ$ . At 10 m from the waist, the beam core has hence expanded to an  $x$ -dimension of 4 m. Dimensions and fields for the three magnets in Fig. 2 are shown in Table I. The calculation confirmed the features of the distribution shown in Fig. 1d.

Although it was convenient to use MARYLIE for optimizing the beamline, a high-order code should be used to accurately predict the particle distribution in phase space. We calculated the particle coordinates at the exit of the octupole using the third-order code MARYLIE, the fifth-order code COSY<sup>2</sup>, and a code that we wrote for the purpose of tracking particles through an octupole. For the extrema of the beam we found large differences between

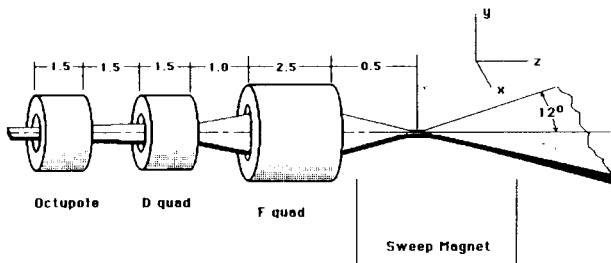


Fig.2. A practical transport line that produces a uniform ribbon beam. Distances are in meters.

TABLE I. PROPERTIES OF LENS ELEMENTS FOR THE BEAMLINE OF FIG. 2

	Octupole	D quad	F quad
Length (m)	1.5	1.5	2.5
Strength	185 T/m <sup>3</sup>	3.0 T/m	4.25 T/m
Pole-tip radius (m)	0.2	0.4	0.4
Pole-tip field (T)	1.5	1.2	1.7

MARYLIE and COSY, suggesting large fifth-order contributions, and smaller differences between COSY and the particle-tracking code, suggesting some seventh-order effects.

In the presence of a duodecapole, use of at least a fifth-order code is mandatory. We employed a particle-tracking code to study the effects of an octupole with a duodecapole component. For a pure octupole, the beam at the exit of the F quad is shown in Fig.3a for an initially Gaussian distribution including particles up to  $5\sigma$ . It can be seen from the figure that not all particles are captured by the core. The effects of combining a duodecapole of strength  $-1500 \text{ T/m}^5$  with the octupole are shown in Fig.3b; all particles within  $5\sigma$  of the initial distribution are now captured.

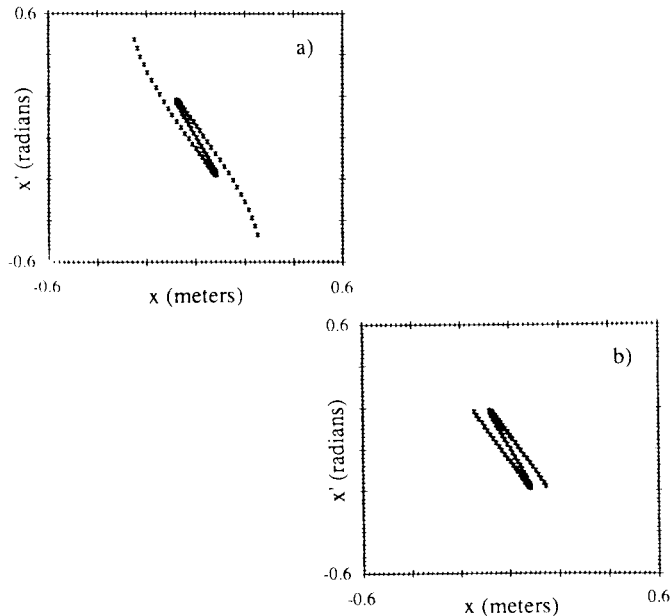


Fig.3. Phase space areas just downstream of the F quad in Fig.2. In a) the transport line was optimized with an octupole, whereas in b) a duodecapole was added. The plots show particles out to  $5\sigma$ . Particles were tracked using a one-dimensional particle tracking program with element settings obtained by optimization using the code MARYLIE.

The addition of space charge to the problem was treated with the particle-tracking code PATH.<sup>3</sup> The results, shown in Fig.4, are insensitive to current. Raising the beam current from 400 mA to 3 A resulted in small distribution changes. We note that while similar third-order effects, caused by space charge forces, are seen in high-intensity beams without the introduction of nonlinear elements, such effects are not evident in our configuration. The long tails in the peaked y-distribution are a consequence of finite-length octupole and finite beam size effects.

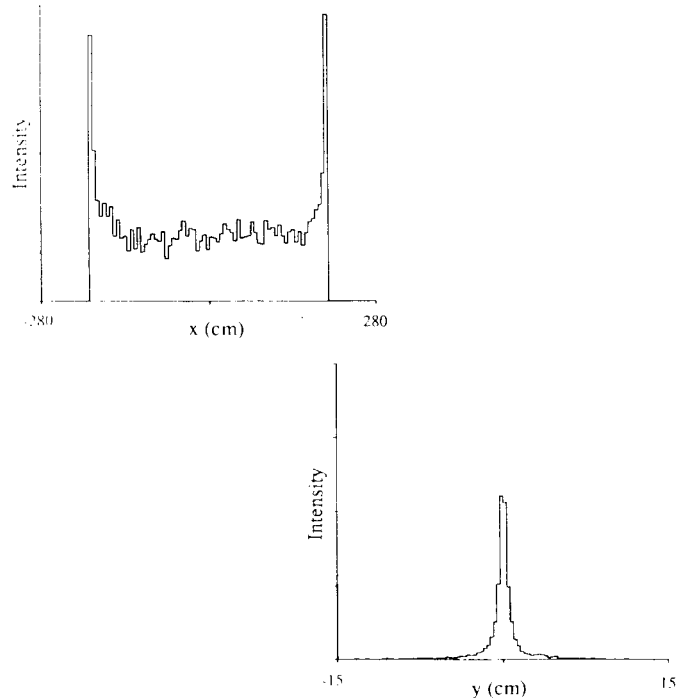


Fig.4. Output intensity distributions for the beamline of Fig.2 obtained using the particle-tracking code PATH on an initially Gaussian beam. The calculation takes into account third-order and space-charge effects. The beam has a 2-GeV energy and a 400-mA current.

For the method outlined above to work, it is not necessary that the initial density distribution be Gaussian. We have successfully flattened initially parabolic distributions.

### Two-Dimensional Flatness

It is tempting to work toward a beam that is two-dimensionally uniform. Toward this goal we have attempted to focus the beam so that it is large in the y-dimension while maintaining a waist in x just after the F quad in Fig.2. Insertion of a nonlinear element at this point duplicates the conditions we have set up for the x-dimension. We have not yet succeeded in producing a two-dimensional version of the distribution in Fig.1d for practical lens parameters. Part of the difficulty is that the beam's x-dimension cannot be made small at the waist as can be seen from Fig.3. The finite x size increases the size of the cross terms in Eq.(1), producing long tails in the final beam. We do not further describe these results in this report.

### Conclusion

The configuration we have described seems suitable to the APT scheme. With the octupole-duodecapole combination,  $5\sigma$  of the beam will be contained in the core. The remaining beam fringes are appreciable ( $0.4 \mu\text{A}$ ) but may be eliminated by upstream scraping. The cusps at the beam extremes contain several percent of the beam

particles and will cause additional heating at the beam-stop edges. This energy can be used effectively to produce neutrons by extending the beam-stop material to the side walls of the target entrance chamber and allowing the beam edges to graze the walls. The vertical sweep magnet is to be placed at the x-waist just after the F quad. Its required aperture is about 50 cm with estimated exterior dimensions of 1.5 by 2.0 m by 1.2 m long. Assuming a 1.5-T peak field, the reactive EMF would be less than 4.5 kV at a 1-Hz sweep rate. These requirements are substantially less than for a raster approach.

Most of our calculations were performed using third-order codes. For a rigorous treatment, the entire beamline should be described to high order. Such calculations will result in somewhat different optimized values for the elements, but no fundamental changes are expected.

The proposed scheme has other possible uses than the APT project. However, it is most workable for highly

expanded beams so that the product of the beam divergence and size is large compared to the original beam emittance. Note also that the beam emittance is greatly enlarged by the process.

#### References

1. D. R. Douglas and Etienne Forest, "A Program for Nonlinear Analysis of Accelerator and Beamline Lattices," *IEEE Trans. Nucl.Sci.* **32** (5), 2311 (1985).
2. M. Berz, H. C. Hoffmann and H. Wollnik, "COSY 5.0 - the Fifth Order Code for Corpuscular Optical Systems," *Nucl. Instrum. and Methods*, **A258**, 402 (1987).
3. J.A. Farrell, "PATH-A Lumped Element Beam Transport Simulation Program with Space Charge," *Proc. of Berlin Conf. on Computing in Accel. Design and Operation*, W. Busse and R. Zelany, Ed., Springer Verlag, Berlin, 267 (1984).